Supplementary Information (SI) for Nanoscale.

Chiral π-Conjugated Polymer Films via Kinetic-Controlled Dip-Coating for Circularly Polarized Light Information Encoding

*Haitao Cheng,[a†] Ke Gao,[b†] Chao Zhang,[a†] Haoze Li,[a] JingRun Yang,[d] Zibo Meng,[a] Liang Jiang,[a] Xiaobo Shang,[*b] Yuchen Wu [c] and Hanfei Gao [*a]*

a. *State Key Laboratory of Bioinspired Interfacial Materials Science, Suzhou Institute for Advanced Research, University of Science and Technology of China, Suzhou, Jiangsu 215123, P. R. China. E-mail: gaohanfei15@mails.ucas.ac.cn.*
b. *State Key Laboratory for Porous Metal Materials, School of Materials Science and Engineering, Xi'an Jiaotong University, Xi'an 710049, P. R. China. E-mail: xiaoboshang@xjtu.edu.cn.*
c. *College of Chemistry, Jilin University, Changchun, 130012, P. R. China*
d. *Department of General Surgery, the First Medical Center of Chinese PLA General Hospital, Beijing, 100853, P. R. China. E-mail: yangjingrun@301hospital.com.cn.*

† H. Cheng, K. Gao and C. Zhang contributed equally.
* Corresponding authors.

Supporting Contents

1.Experimental Methods

Synthesis Chiral Polymers

All reagents and deuterated solvents were used as purchased without further purification. Compounds 2,6-dibromonaphthalene-1,4,5,8-tetracarboxylic dianhydride (NDA-Br_2), 2-octanamine and 2,5-bis(trimethylstannyl)thiophene purchased from commercial suppliers. (*S*)-NDI2MH-Br_2 compounds were prepared according to the literature procedure.[16]

For the synthesis of chiral polymer poly{[*N*,*N*'-bis(1-methylheptyl)-1,4,5,8-naphthalene diimide-2,6-diyl]-*alt*-5,5'-(2,2'-thiophene)} [(*S*)-P(NDI2MH-T)]: A mixture of (*S*)-NDI2MH-Br_2 (0.35 g, 0.54 mmol), 2,5-bis(trimethylstannyl)thiophene (0.22 mg, 0.54 mmol) and $Pd(PPh_3)_2Cl_2$ (37.89 mg, 0.05 mmol) in anhydrous toluene (25 mL) were stirred under argon at 90 ℃ for 4 days. Bromobenzene (0.2 mL) was then added and the reaction mixture was maintained at 90 ℃ for an additional 12 hours. Upon cooling to room temperature, a solution of potassium fluoride (1.0 g) in water (2.0 mL) was added. This mixture was stirred at room temperature for 2 h before it was extracted with chloroform (60 mL × 3). Organic layers were combined, washed with brine (50 mL × 3), then water (50 mL × 3), dried over anhydrous sodium sulfate, and concentrated on a rotary evaporator. The residue was redissolved with a small amount of chloroform and precipitated in methanol three times. The obtained dark blue solid product was purified by Soxhlet extraction with acetone for 72 h. The remaining solid residue was redissolved in chloroform (20 mL) and the resulting mixture was heated to boil. Upon cooling to room temperature, the chloroform solution was filtered through a 5 μm filter, and the filtrate was added slowly to methanol (250 mL). The precipitates were collected by filtration, washed with methanol, and dried in vacuum, leading to afford (*S*)-P(NDI2MH-T) as dark blue solid (yield 42%).

Substrate Wettability Modification

Clean silicon wafers were first cut into 1 cm × 1 cm squares using a diamond scribe and a steel ruler. The pieces were then ultrasonically cleaned successively in ethanol, acetone, and ultrapure water for 20 minutes each. After cleaning, the silicon substrates were dried under a stream of nitrogen and stored as clean substrates for further use.

For wettability modification, a chemical vapor deposition method was employed. The clean silicon substrates were first treated with plasma cleaning and then placed inside a vacuum desiccator. Using a micropipette, 200 μL of the modifying agent was dispensed evenly along the inner wall of the desiccator, allowing the reagent to flow down the wall. The desiccator was sealed, and vacuum was applied for 30 minutes. Subsequently, the desiccator was transferred to an oven and heated at 110 °C for 3 hours. After heating, the desiccator was removed, and the modified silicon substrates were obtained.

Film Preparation via Dip-Coating

(*S*)-P(NDI2MH-T) polymer was dissolved in chloroform to prepare solutions with concentrations of 0.5, 1, 2, and 5 mg/mL. Si/SiO_2 substrates were cleaned by sequential ultrasonication in ethanol, acetone, and ultrapure water for 20 minutes each, followed by drying under a nitrogen stream.

Each polymer solution was placed in a separate small vial and thermally equilibrated on a hot plate set at 25, 35, 45, or 55°C. A silicon substrate was held vertically and immersed into the solution at a controlled depth for a fixed duration, then withdrawn at a constant speed to form a thin film. By varying the substrate surface modification, solution concentration, and coating temperature as three independent variables, a series of dip-coated films were systematically prepared.

Fabrication of Organic Photodetector Devices

Organic photodetectors with a bottom-gate, top-contact configuration were fabricated. Initially, gold source and drain electrodes were patterned on silicon/silicon dioxide substrates via photolithography. Subsequently, a polymer film serving as the n-type semiconductor was deposited onto the substrate using the dip-coating method described above, thereby completing the organic photodetector device.

Optoelectronic characterization

The performance of the photodetector devices was characterized by a Keysight B1500A semiconductor parameter analyzer coupled with a Lake Shore manual probe station and a 365 nm LED driven by a Thorlabs DC2200 current source supplied the illumination at room temperature under vacuum conditions. its incident power was calibrated with a silicon photodiode (Thorlabs S130C), a linear polarizer (Thorlabs, WP25M-UB, America) and a quarter-wave plate (Thorlabs, AQWP05M-600, America). The modification of the silicon template was demonstrated by a contact-angle system (Dataphysics, OCA 20, Germany) through measuring the static contact angle (CA) at different positions of the silicon template.

Materials characterization

The microstructures of (*S*)-P(NDI2MH-T) thin films were observed using a DP80 microscope (Olympus, Japan). UV-vis absorption and circular dichroism (CD) spectra were measured on a J-815 CD spectrometer (JASCO, Japan). Morphological images were acquired by a SU8000 scanning electron microscope (Hitachi High-tech, Japan). Atomic force microscopy (AFM) imaging was performed on an ICON2-SYS atomic force microscope (Bruker, Germany).

Estimation of Chiro-Optical and Electrical Properties

The field-effect mobility (μ) and the threshold voltage (V_T) were estimated in the saturation regime (V_{DS} = 60 V) with the following equation:

$$I_D = \frac{W}{2L}\mu C_i(V_G - V_T)^2 \quad \text{(S1)}$$

where I_D is the drain current, W and L are the semiconductor channel width and length, respectively. μ is the mobility and C_i is the capacitance per unit area of the gate dielectric. V_G and V_T are the gate voltage and threshold voltage, respectively.

In order to investigate photosensitivity for devices, photoresponsivity (R) was calculated from transfer characteristics coupled with light irradiation. The R values are typically defined by the following equations:

$$R = (I_{light} - I_{dark})/W_{inc}S \quad \text{(S2)}$$

where W_{inc} the incident illumination power on the channel of the device, S is channel area, I_{light} the drain current under illumination, and I_{dark} the drain current in the dark, respectively.

$$D^* = R\sqrt{S}/\sqrt{2eI_{dark}} \quad \text{(S3)}$$

To quantitatively evaluate the CPL detection selectivity of devices, the asymmetry factor of the photocurrent (g_{ph}) was calculated. The expression for extracting g_{ph} is:

$$g_{ph} = 2(I_{ph}^L - I_{ph}^R) / (I_{ph}^L + I_{ph}^R) \quad \text{(S4)}$$

Computational Methods

The single molecule structures underwent optimization using density functional theory (DFT) in a vacuum environment, utilizing Gaussian 16 software. Following geometry optimization, vibrational frequencies were calculated, with no imaginary frequency was found. The UV-vis absorption and circular dichroism spectra, along with the electric and magnetic transition dipole moments, were carried out through time-dependent density functional theory (TD-DFT) method based on the optimized S0 geometry, the lowest 60 states were taken into consideration. For all of the aforementioned DFT calculations, the B3LYP functional was used in conjunction with a 6-31G(d) basis set.

2.Additional Figures

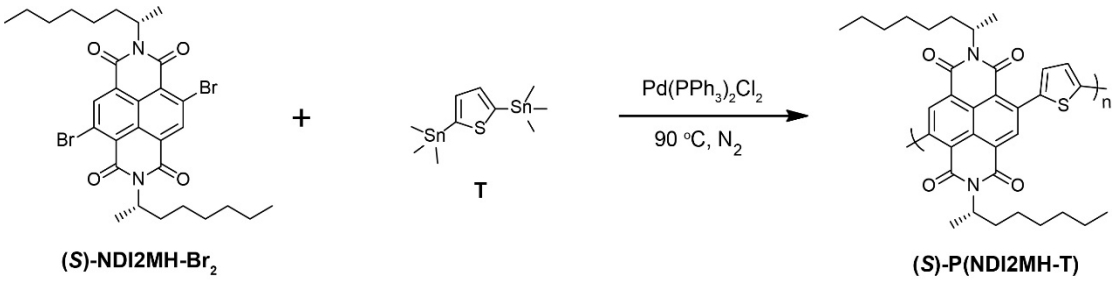

Fig. S1 (*S*)-P(NDI2MH-T) synthetic route.

(*S*)-P(NDI2MH-T): ^{1}H NMR (400 MHz, $CDCl_3$, 298 K): δ: 8.93-8.92 (m, br, 2 H), 7.44 (s, br, 2 H), 5.25-5.20 (m, br, 2 H), 2.20-1.24 (m, br, 26 H), 0.84-0.80 (m, br, 6 H).

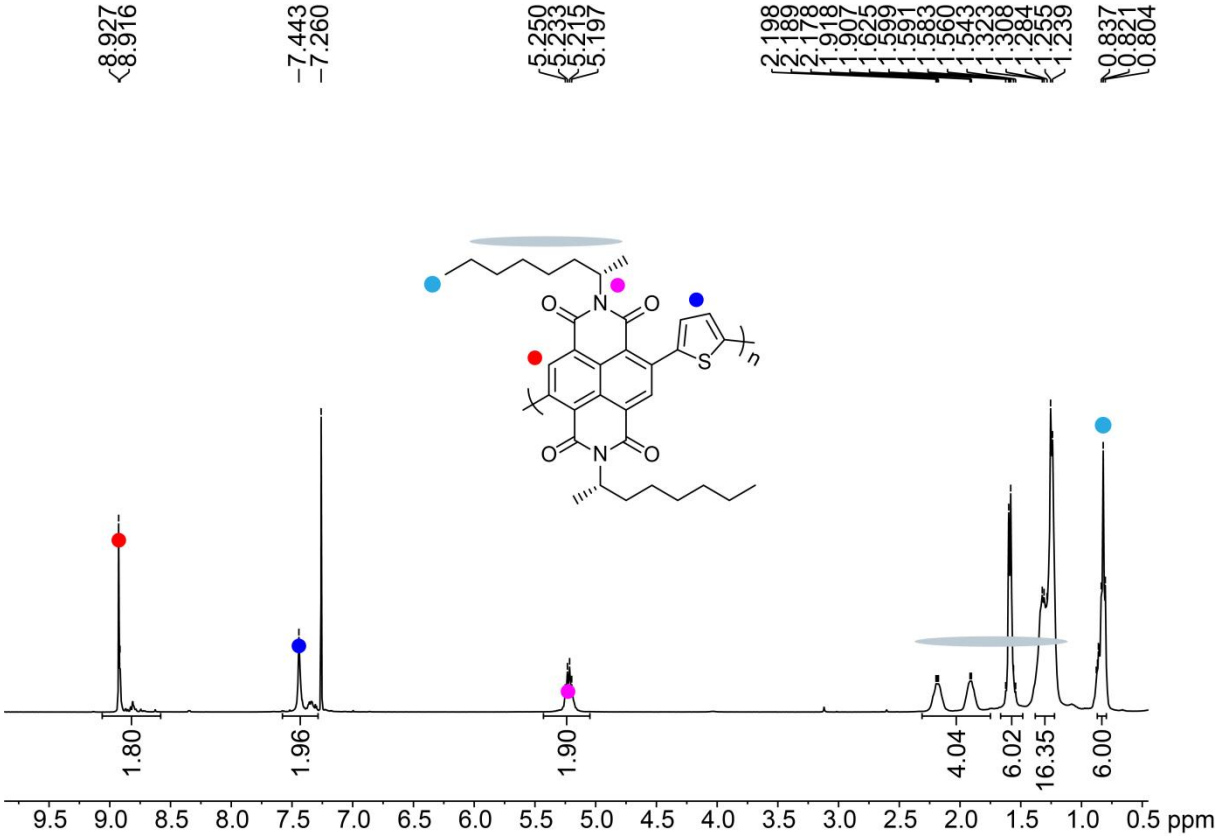

Fig. S2 ^{1}H NMR spectra (400 MHz, $CDCl_3$, 298 K) recorded for (*S*)-P(NDI2MH-T).

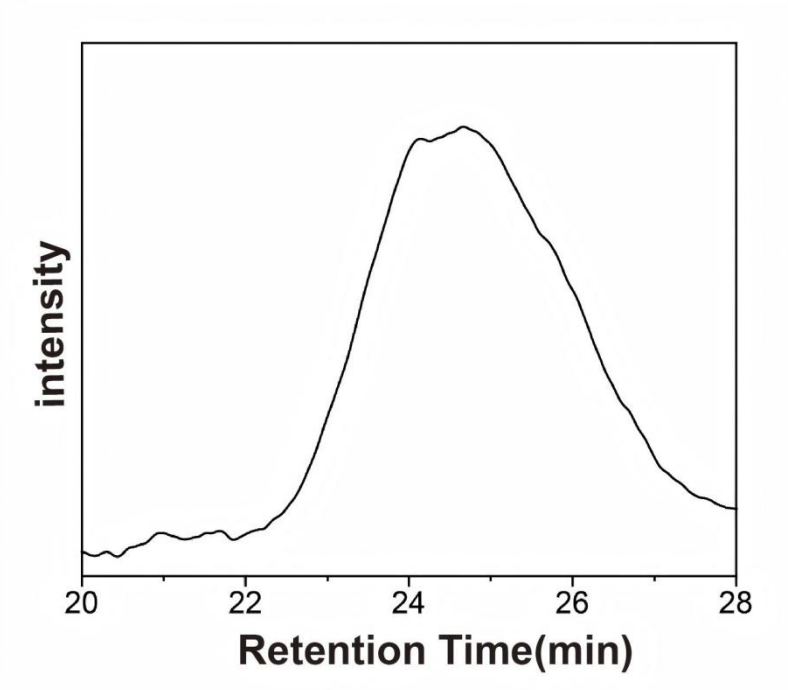

Fig. S3 Gel permeation chromatography (GPC) for (*S*)-P(NDI2MH-T).

Table S1. GPC results of (*S*)-P(NDI2MH-T).

M_n (g mol^{-1})	M_w (g mol^{-1})	M_z (g mol^{-1})	M_{z+1} (g mol^{-1})	M_η (g mol^{-1})	$Đ$
16689	26787	38486	49279	25157	1.61

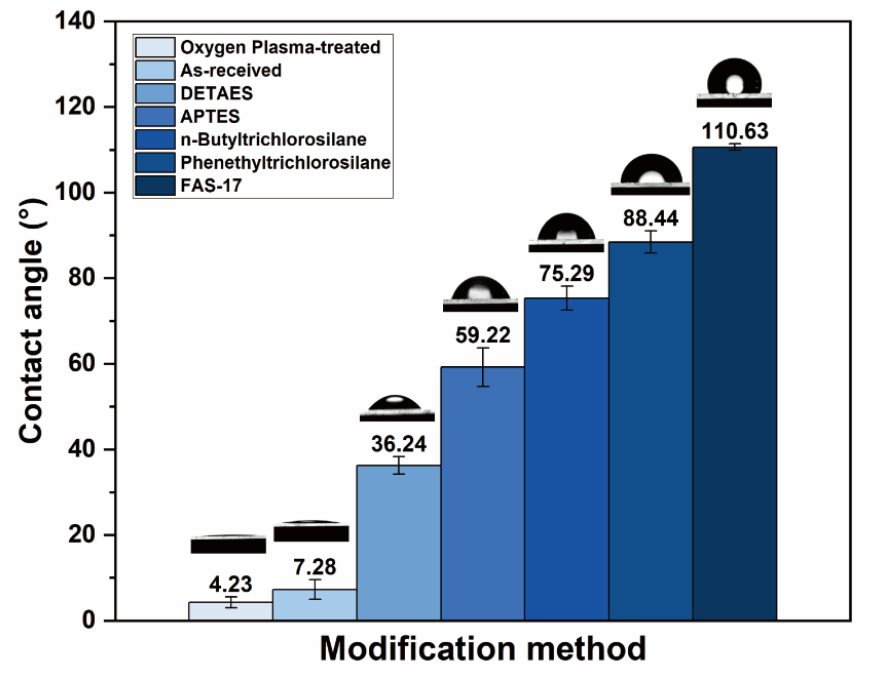

Fig. S4 Contact Angles for Substrates Modified with Different Agents.

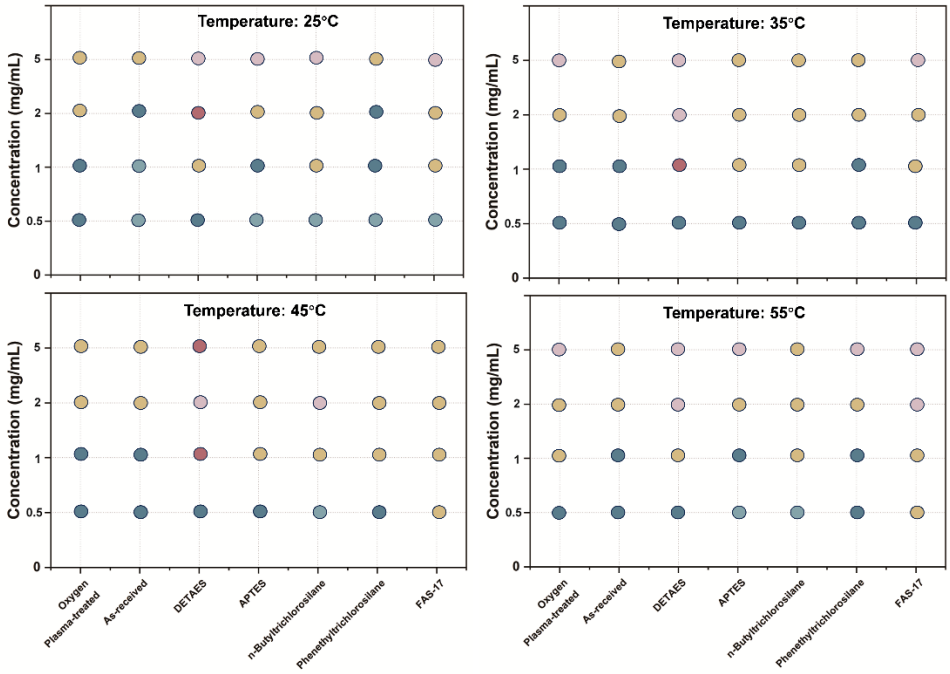

Fig. S5 Statistical analysis of film quality of (*S*)-P(NDI2MH-T) films obtained by dip-coating at different solution concentrations on substrates with varying wettabilities at the same temperature.

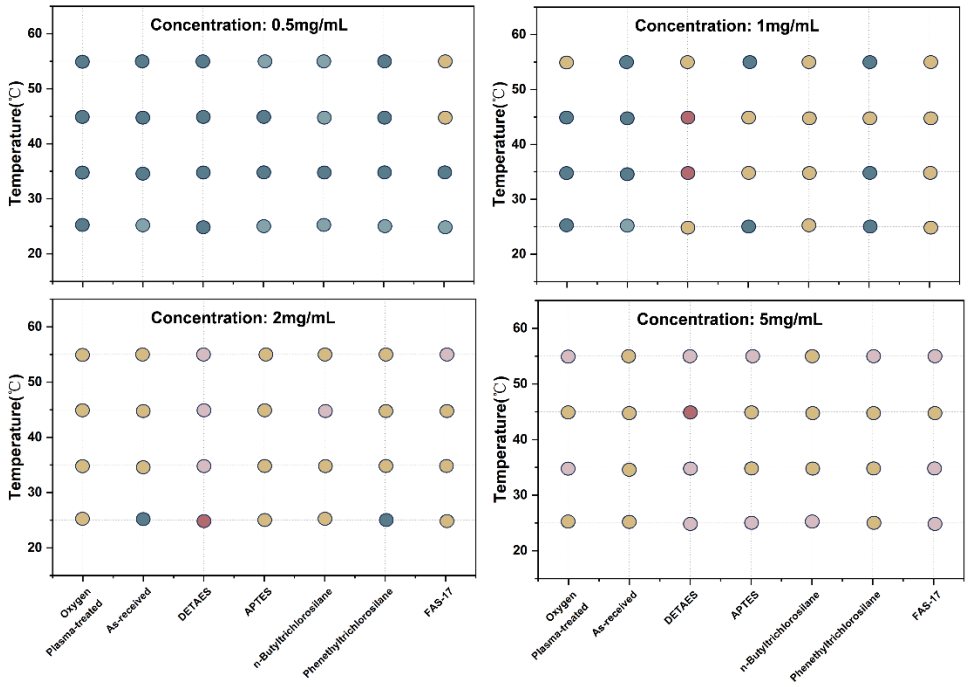

Fig. S6 Statistical chart of film quality prepared by dip-coating from (*S*)-P(NDI2MH-T) solutions at different temperatures and on substrates with varying wettabilities, at the same concentration.

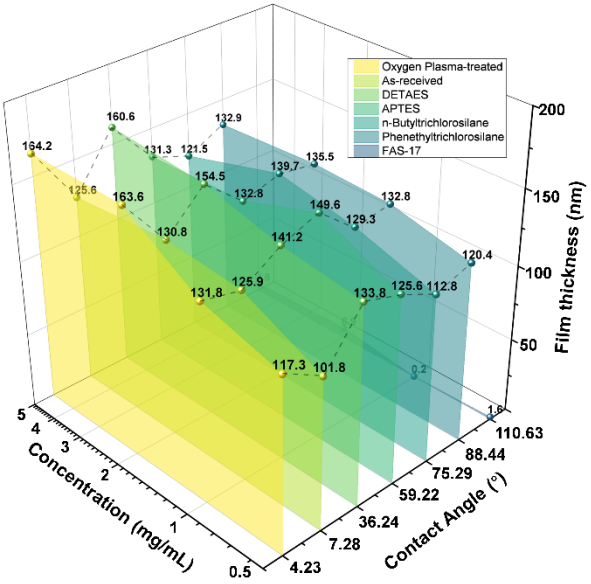

Fig. S7 Statistical distribution of film thicknesses of (*S*)-P(NDI2MH-T) films prepared by dip-coating at different solution concentrations on substrates with varying contact angles at 35 °C.

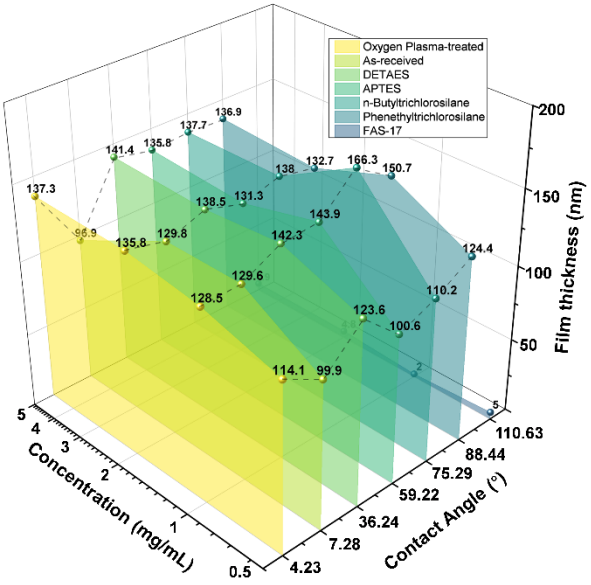

Fig. S8 Statistical distribution of film thicknesses of (*S*)-P(NDI2MH-T) films prepared by dip-coating at different solution concentrations on substrates with varying contact angles at 45 °C.

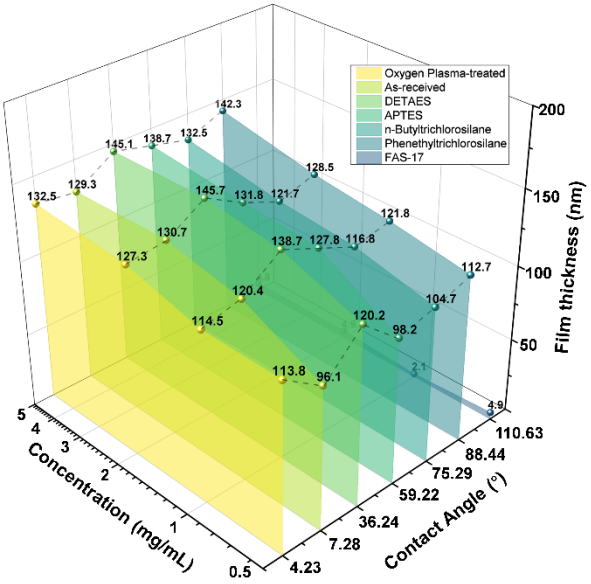

Fig. S9 Statistical distribution of film thicknesses of (*S*)-P(NDI2MH-T) films prepared by dip-coating at different solution concentrations on substrates with varying contact angles at 55 °C.

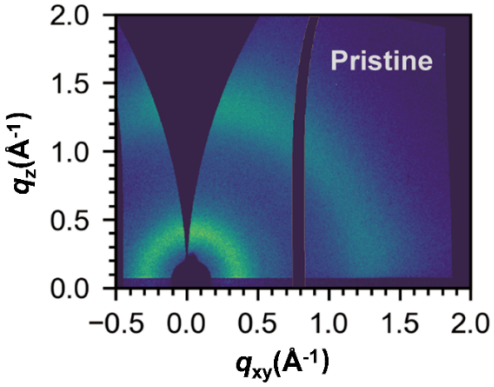

Fig. S10 The 2D GIWAXD patterns of pristine (*S*)- P(NDI2MH-T) film.

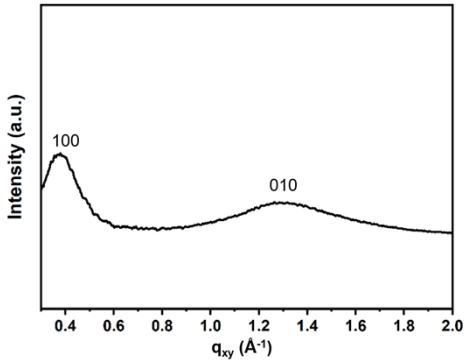

Fig. S11 GIWAXS scattering patterns of (*S*)-P(NDI2MH-T) in the q_{xy} direction.

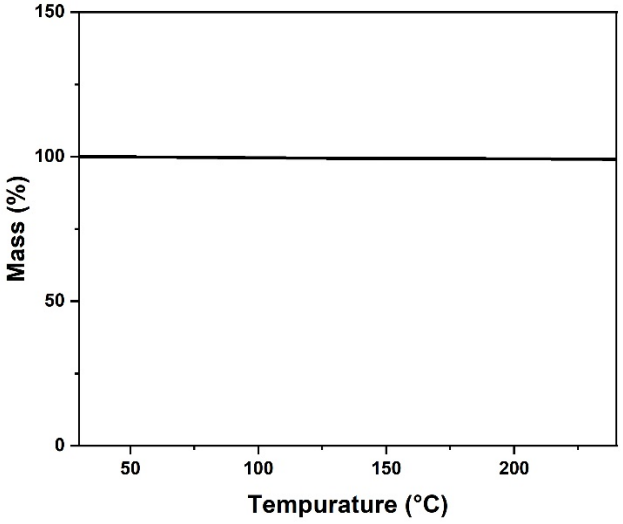

Fig. S12 Thermogravimetry (TGA) for (*S*)-P(NDI2MH-T) film.

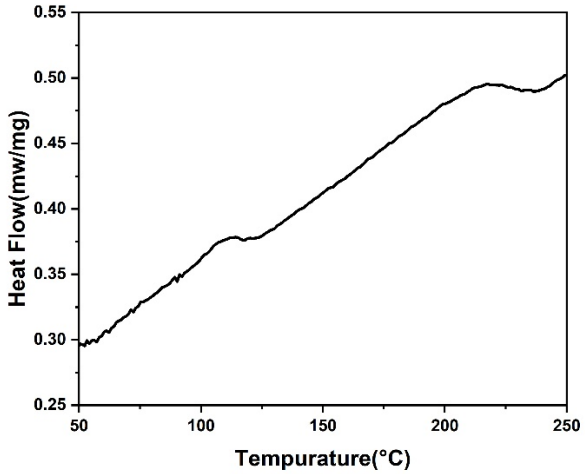

Fig. S13 Differential scanning Calorimetry (DSC) for (*S*)-P(NDI2MH-T) film.

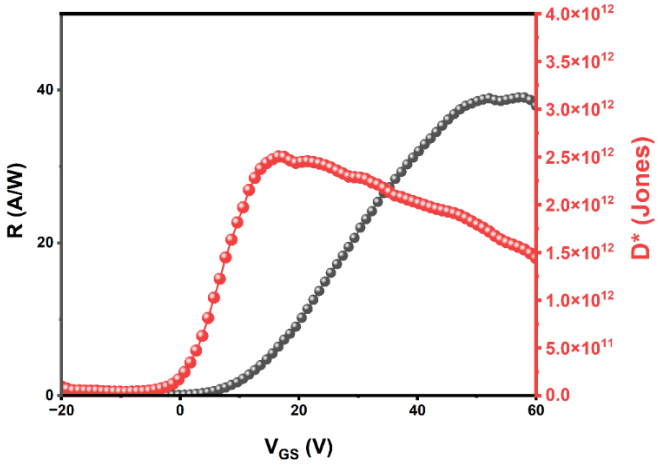

Fig. S14 *R* and *D** of the (*S*)-P(NDI2MH-T) thin-film photodetector.

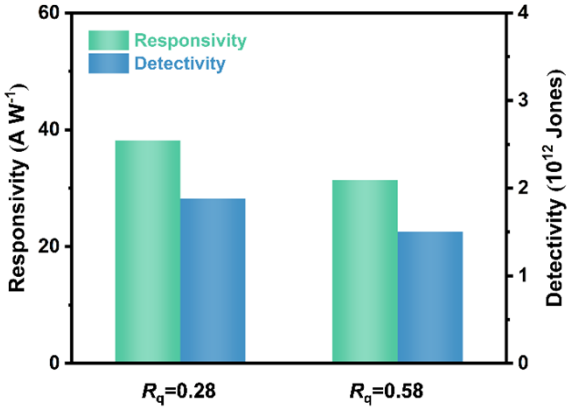

Fig. S15 Comparison of responsivity and detectivity for film devices with lower roughness (R_q = 0.28) and higher roughness (R_q = 0.58) achieved through kinetic control.

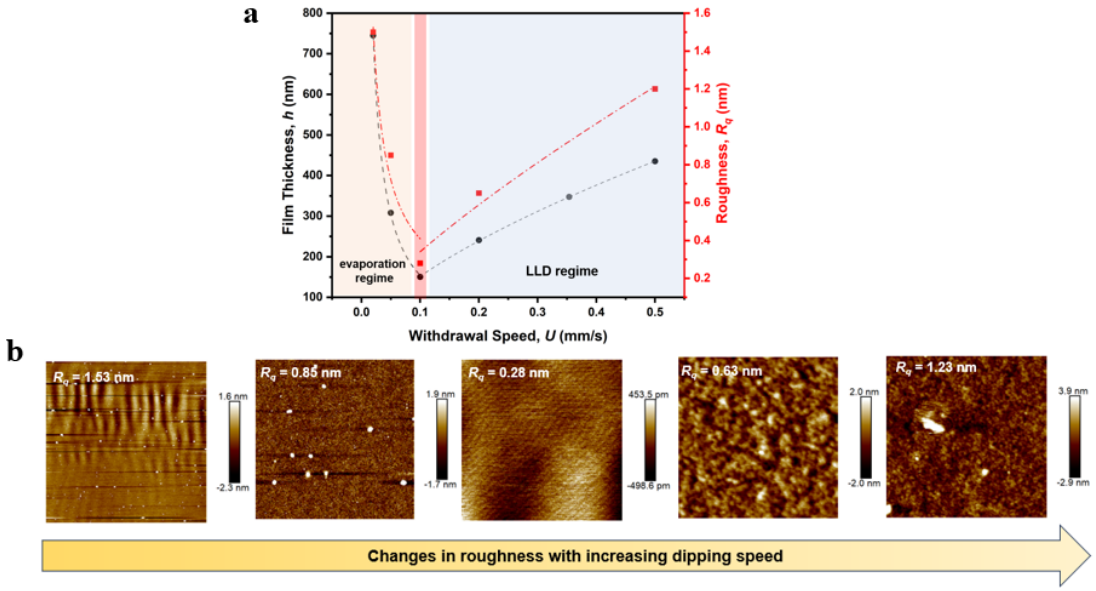

Fig. S16. (a) Quantitative scaling relationship between the withdrawal speed (U) and the resulting film thickness (h, blue circles) and surface roughness (R_q, red squares) of the (*S*)-P(NDI2MH-T) films. (b) Corresponding atomic force microscopy (AFM) height images of the (*S*)-P(NDI2MH-T) films prepared at different withdrawal speeds: 0.02, 0.05, 0.1, 0.2, and 0.5 mm/s.

Table S2. Quantitative criteria and structural features for the morphological classification of dip-coated (*S*)-P(NDI2MH-T) films.

Morphology Category	Surface Coverage (%)	Experimental Reference Roughness Range (R_q, nm)
Continuous and Smooth	> 99%	<0.5
Particulates	90% - 99%	0.5 – 1.2

Cellular structure	75% - 90%	0.8 – 2.5
Discontinuous islands	40% -75%	0.9 – 3.5
Filamentary residue	< 40%	-

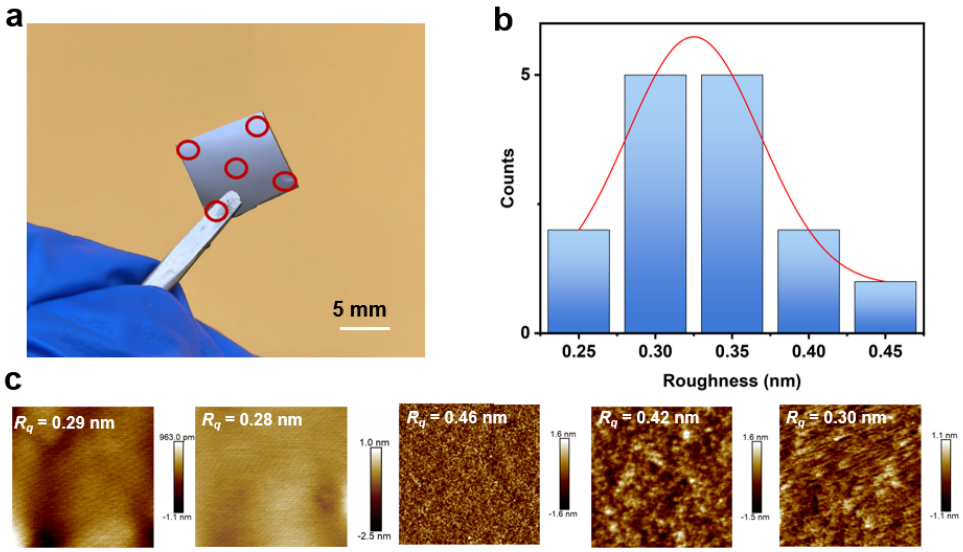

Fig. S17 (a) Schematic diagram illustrating the locations of five sampling points on a silicon wafer sample. (b) and (c) Statistical distribution of roughness and topographic images obtained from independent AFM scans of the optimized (S)-P(NDI2MH-T) films.

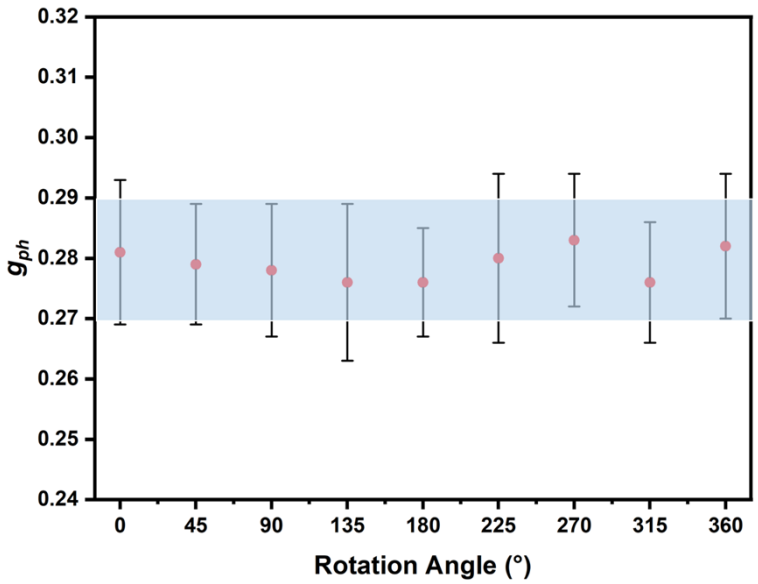

Fig. S18 In-plane angle-independent CPL response of the device**.**

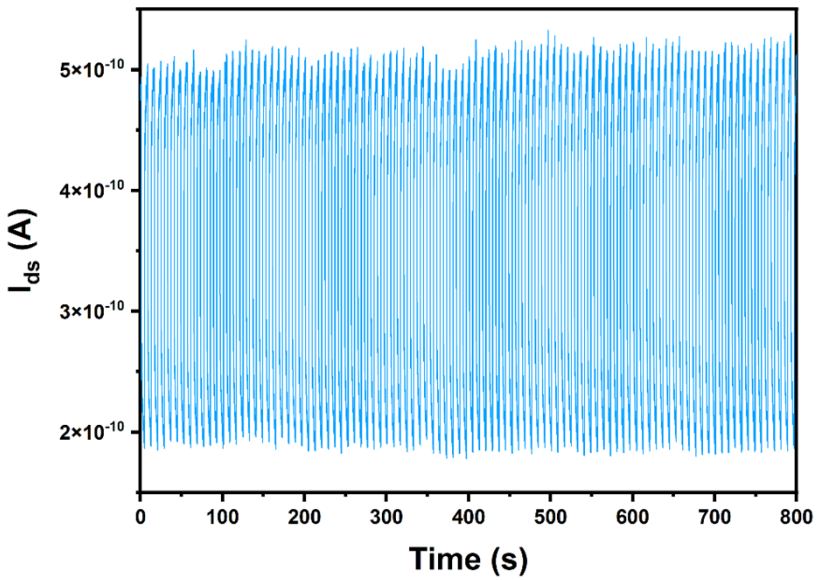

Fig. S19 Long-term photo-switching stability. Time-resolved photocurrent (I–t) response of the (*S*)-P(NDI2MH-T) based device under repetitive on/off illumination cycles (λ = 365 nm) for 800 s. The consistent photo-response over 100 cycles demonstrates the operational robustness and reliability of the device for stable signal encoding.

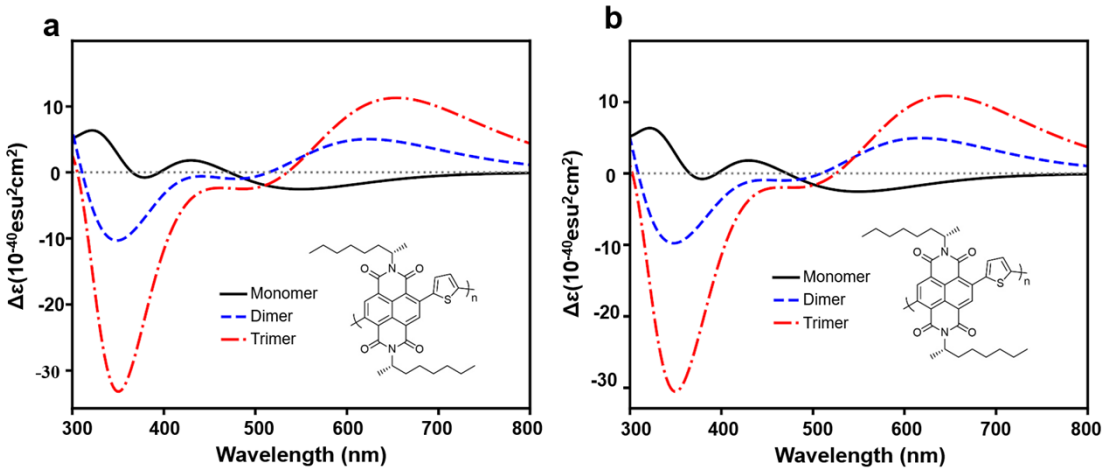

Fig. S20 Calculated CD spectra of the monomer, dimer, and trimer models in (a) chloroform and (b) dichloromethane using TD-DFT calculations. The evolution from monomer to trimer illustrates the emergence of bisignate signals and a red-shift in the absorption peaks, which bridge the gap between intrinsic molecular chirality and the chiroptical responses observed in polymer films.

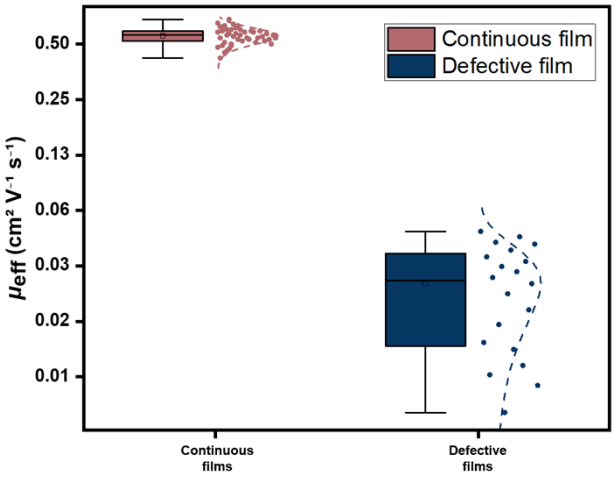

Fig. S21 Statistical box plot of the effective mobility (μ_{eff}) for functional devices.

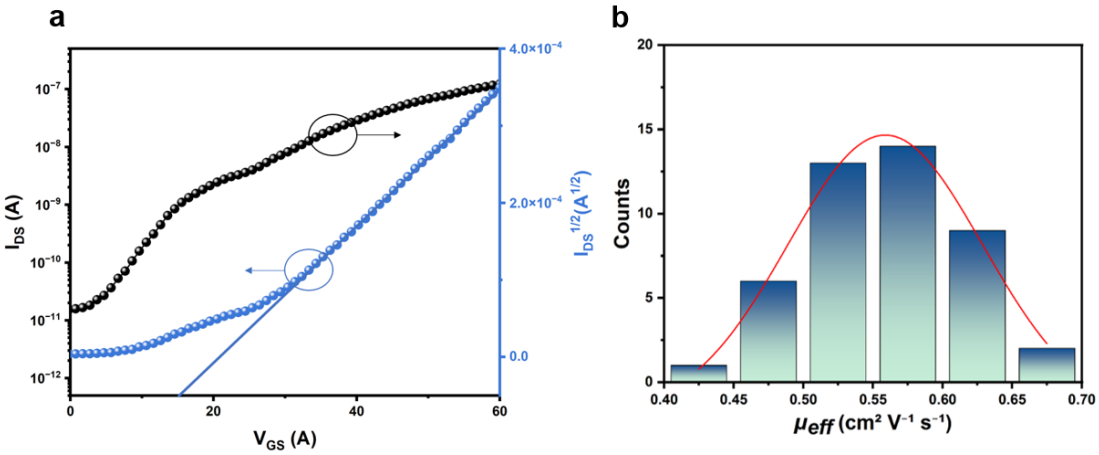

Fig. S22 (a) transfer curve of the device based on thin film device. (b) Statistical distribution of the effective field-effect mobility (μ_{eff}). The histogram represents the mobility distribution for 45 independent OFET devices fabricated across 5 different batches.